THE ROLE OF GAS IN THE MERGING OF MASSIVE BLACK HOLES IN GALACTIC NUCLEI. II. BLACK HOLE MERGING IN A NUCLEAR GAS DISK

ANDRÉS ESCALA
Department of Astronomy, Yale University, New Haven, CT 06520-8101; and Departamento de Astronomía,
Universidad de Chile, Casilla 36-D, Santiago, Chile

RICHARD B. LARSON AND PAOLO S. COPPI
Department of Astronomy, Yale University, New Haven, CT 06520-8101

AND

DIEGO MARDONES
Departamento de Astronomía, Universidad de Chile, Casilla 36-D, Santiago, Chile

ABSTRACT

Using high-resolution SPH numerical simulations, we investigate the effects of gas on the in-spiral and merger of a massive black hole binary. This study is motivated by the very massive nuclear gas disks observed in the central regions of merging galaxies. Here we present results that expand on the treatment in a previous work by studying models in which the gas is in a disk. We run a variety of models, ranging from simulations with a relatively smooth gas disk to cases in which the gas has a more clumpy spatial distribution. We also vary the inclination angle between the plane of the binary and the plane of the disk, and the mass ratio between the MBHs and the gaseous disk. We find that, as in our previous work, in the early evolution of the system the binary separation diminishes mainly due to dynamical friction exerted by the background gas, and in the later stages the gaseous medium responds by forming an ellipsoidal density enhancement whose axis lags behind the binary axis. This offset produces a gravitational torque on the binary that causes continuing loss of angular momentum and is able to reduce the separation to distances at which gravitational radiation is efficient. The main difference is that between these two regimes we now find a new transition regime that was not apparent in our previous paper, in which the evolution is temporarily slowed down when neither of these mechanisms is fully effective. In the variety of simulations that we perform, we find that the coalescence timescale for the MBH binary varies between 5×10^6 and 2.5×10^7 yr for typical ULIRGs. For MBHs that satisfy the observed "m-σ_c" relation, our simulations suggest that in a merger of galaxies that have at least 1% of their total mass in gas, the MBHs will coalesce soon after the galaxies merge.

Subject headings: black hole physics — cosmology: theory — galaxies: evolution — galaxies: nuclei — hydrodynamics — quasars: general

1. INTRODUCTION

The possibility of massive black hole (MBH) mergers follows from two widely accepted facts: that galaxies merge and that every galaxy with a significant bulge hosts an MBH at its center (Richstone et al. 1998). This problem was first considered by Begelman et al. (1980) in a study of the long-term evolution of a black hole binary at the center of a dense stellar system. Initially, dynamical friction brings the two black holes toward the center of the system. The resulting binary MBH continues to shrink via three-body interactions with the surrounding stars, but three-body interactions tend to eject stars from the central region, causing the merger eventually to stall, unless some additional mechanism is able to extract angular momentum from the MBH binary.

The possible additional mechanism that extracts angular momentum from the binary is very likely to be gasdynamical in origin. Observations of gas-rich interacting galaxies such as the ultraluminous infrared galaxies (ULIRGs) indicate that large amounts of gas are present in the central regions of merging galaxies (Sanders & Mirabel 1996). This massive nuclear gas concentration has an important influence on the evolution of any central MBH binary that forms following a galaxy merger. Since the gas is strongly dissipative, unlike the stars, it is expected to remain concentrated near the center and thus to play a continuing

role in driving the evolution of a central binary MBH. Our aim is to study numerically the role of massive nuclear gas clouds in driving the evolution of a binary MBH.

In a previous paper (Escala et al. 2004, hereafter Paper I) we studied numerically the role of a massive spherical gas cloud in driving the evolution of a binary MBH. We followed the evolution of the binary through many orbits and close to the point at which gravitational radiation becomes important. In Paper I, we presented results for a relatively simple idealized case in which the gas is assumed to be supported by a high virial temperature, so that the gas retains a nearly spherical and relatively smooth distribution. We found that in the early evolution of the binary, the separation decreases due to the dynamical friction exerted by the background gas. In the later stages, when the binary dominates the gravitational potential in its vicinity, the medium responds by forming an ellipsoidal density enhancement whose axis lags behind the binary axis, and this offset produces a gravitational torque on the binary that causes continuing loss of angular momentum and is able to reduce the binary separation to distances at which gravitational radiation is efficient. Assuming typical parameters from observations of ULIRGs, we predicted that a black hole binary will merge within 10^7 yr.

The model presented in Paper I is relatively idealized, and as we describe in § 2, observations suggest that the gas in merging systems is in a rotating nuclear disk. In this paper, we study

numerically the role of a massive gas disk, like those seen in the central regions of ULIRGs, in driving the evolution of a binary MBH. We start our simulations when a pair of MBHs is in the violently relaxed core of a newly merged galaxy and with the massive gas disk already settled. The same approach was used in a similar numerical study (Taniguchi & Wada 1996) that was focused on the response of a nuclear gas disk to the presence of an MBH binary. This approach is supported by larger scale simulations of merging galaxies with MBHs (Kazantzidis et al. 2005). Our aim is to explore the physical processes that are relevant in the evolution of an MBH binary after a merger of galaxies. For that purpose, we run a variety of models ranging from simulations with a relatively smooth gas disk to cases in which the gas has a more clumpy spatial distribution. We also vary the inclination angle between the plane of the binary and the plane of the disk and the mass ratio between the MBHs and the gaseous disk. We follow the evolution of the binary through many orbits and close to the point at which gravitational radiation becomes important.

We start with a review of the properties of the inner regions of merging galaxies in § 2. We continue with a description of the assumed initial conditions and the model setup in § 3. In § 4 we study the evolution of a binary MBH in a massive gas disk, exploring the parameters that may be relevant for the coalescence of the binary MBH. In § 5 we study the final coalescence of the binary MBH using higher resolution simulations. In § 6 we study the criteria for opening a circumbinary gap and the implications for the "m-σ_c" relation. Finally, our conclusions are presented in § 7.

2. GAS IN THE NUCLEI OF MERGING GALAXIES

Observational and theoretical work both indicate that large amounts of gas can be present in the central regions of interacting galaxies and that this gas can be a dominant component of these regions. Numerical simulations show that in a merger of galaxies containing gas, much of the gas can be driven to the center by gravitational torques that remove angular momentum from the shocked gas (Barnes & Hernquist 1992, 1996; Mihos & Hernquist 1996); as a result, more than 60% of the gas originally present in the merging galaxies can end up in a very massive nuclear disk with a radius of several hundred parsecs (Barnes 2002). Observations of gas-rich interacting galaxies such as the ULIRGs confirm that their central regions often contain massive and dense clouds of molecular and atomic gas whose masses are comparable to the total gas content of a large gas-rich galaxy (Sanders & Mirabel 1996).

Downes & Solomon (1998, hereafter DS98), using CO interferometer data, show that the molecular gas in ULIRGs, at subarcsecond resolution, is in rotating nuclear disks. These molecular disks are highly turbulent, with typical velocity dispersions of $\sigma = 100$ km s^{-1}. DS98 modeled the CO luminosity as coming mostly from a relatively low-density phase with a gas kinetic temperature in the range ~ 65–100 K. This "low-density" gas is in a smooth medium and not in self-gravitating clouds, and has an average density of 10^3 cm^{-3}. DS98 estimate that only $\sim 10\%$ of the gas is in highly opaque and dense (10^5 cm^{-3}) self-gravitating clouds that are stable against tidal forces, although the exact fraction is still unclear. The derived total gas mass is high, typically 5×10^9 $M_\odot$, which is similar to the mass of molecular clouds in a large, gas-rich spiral galaxy. However, the total mass in molecular gas is still small compared to the dynamical mass derived from the rotation curve, the ratio of gas mass to enclosed dynamical mass being about $M_{\rm gas}/M_{\rm dyn} = 1/6$. In addition to these multiphase nuclear disks, DS98 also found exceptionally massive

clumps with ongoing extreme starburst activity having characteristic sizes of only 100 pc, with about 10^9 $M_\odot$ of gas and an IR luminosity of 3×10^{11} $L_\odot$ from recently formed OB stars.

Since ULIRGs are characterized by an ongoing starburst, feedback effects from star formation may play a major role in determining the physics of the interstellar medium (ISM). The main feedback effects on the gas arise from massive stars and include stellar winds, supernova explosions, and the effect of radiation pressure. Recently, Wada and collaborators have made some attempts to model this complex environment including all the relevant feedback effects (Wada & Norman 2001; Wada 2001). They found a multiphase ISM in which substructure is continuously formed and destroyed, but it reaches a quasi–steady state that is characterized by a network of cold ($T < 100$ K) dense clumps and filaments embedded in a hot ($T > 10^6$ K) diffuse medium.

3. MODEL SETUP

Having reviewed the observations of molecular gas in ULIRGs, we now describe our approach to modeling the complex gaseous environment in the inner regions of merging galaxies.

In our model, the gas is distributed in a rotating disk with a Mestel surface density profile (Mestel 1963),

$$\Sigma_{\rm gas}(R) = \frac{\Sigma_0 R_0}{R}, \qquad (1)$$

and it is initially distributed uniformly between $z = \pm 0.5$. In our simulations, we use the following units: [mass] = 5×10^9 $M_\odot$, [time] = 2.5×10^5 yr, [velocity] = 156.46 km s^{-1}, and [distance] = 40 pc. In these units, which represent the physical conditions in the inner regions of an ULIRG, the gravitational constant G is 22.0511, the disk radius is 10, and the total gas mass is 1.

In addition to the gaseous disk, in this paper we include a stellar bulge that stabilizes the disk and plays an important role in the evolution of the MBH binary when the binary is out of the plane of the disk. The bulge is modeled using a Plummer law (Plummer 1911),

$$\rho(r) = \frac{3}{4} \frac{M_{\rm bulge}}{a^3} \left(1 + \frac{r^2}{a^2}\right)^{-5/2}, \qquad (2)$$

where $a = 5$ is the core radius and $M_{\rm bulge}$ is the total mass of the bulge. The mass of the bulge within $r = 10$ is 5 in the just-mentioned units. This choice was made to satisfy the observed rotation curves (DS98), which imply that the total gaseous mass is 1/6 of the dynamical mass. We model the bulge with a collection of 100,000 collisionless particles, with a gravitational softening length of 0.1. For the gaseous disk, we employ 235,331 smoothed particle hydrodynamics (SPH) particles, and the softening length is also 0.1.

In modeling the gas disk, we do not attempt a fully realistic description, which would include turbulence, star formation, feedback effects, etc. Instead, we adopt a more phenomenological approach, intended to reproduce approximately the observed properties of gas disks in merging galaxies. As noted in § 2, these observed disks are turbulent and contain a smooth intercloud component as well as massive self-gravitating clouds. Because isothermal equations of state have often been used to model gas disks, we first considered a cold massive disk ($c_S = 0.01$, $M_{\rm disk} = 1$) with an isothermal equation of state. This disk is gravitationally unstable ($Q \ll 1$), and therefore it soon fragments into clumps. As is true generally for an isothermal

Run	M_{BH}/M_{gas}	Angle (deg)	K
A....................	0.01	0	0.4665
B....................	0.01	0	0.933
C....................	0.01	0	1.3995
D....................	0.01	0	2.3325
E....................	0.01	22.5	0.933
F	0.01	45	0.933
G....................	0.01	67.5	0.933
H....................	0.03	0	0.933
I	0.05	0	0.933
J....................	0.1	0	0.933
K....................	0.3	0	0.933
L	0.5	0	0.933

equation of state, these clumps undergo a runaway collapse toward infinite central density, and in the simulations, this collapse stops only at the gravitational softening length. The resulting simulated clumps have densities many orders of magnitude higher than the observed ones (DS98), and therefore they are unrealistic.

In this unrealistic model, we find that the MBHs interact violently and chaotically with the clumps, but in most cases they end up at the center, where they continue to lose angular momentum by interaction with a central massive clump, qualitatively as in Paper I.

In reality, the clumps will rapidly form stars, and feedback processes from starburst activity may tend to halt their runaway collapse. The feedback effects and the detailed internal evolution of the clumps are very difficult to model numerically, so we adopt a simple parameterized equation of state that allows us to represent a clumpy medium with the observed range of densities. Such a model should provide a better description for our purposes than the isothermal model with its unrealistic densities. The detailed structure and evolution of the clumps is not important for our problem, because the gravitational drag effect depends strongly on only one property of the gas, its local density. Our aim is to model only the most important effects controlling the decay rate of the MBH binary, and for this we do not require a fully realistic description of the gas.

In order to prevent the runaway collapse of the clumps, we adopt a simple polytropic equation of state,
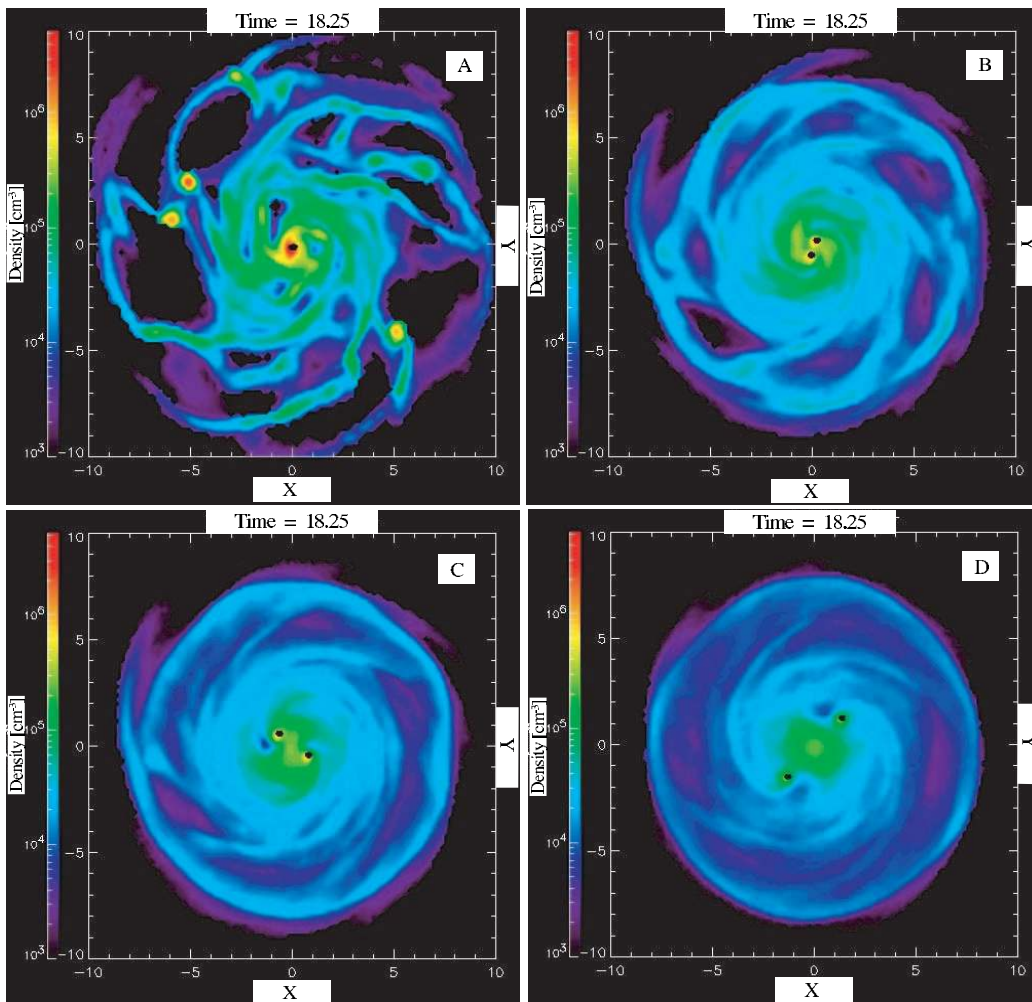
$$P = K\rho^{\gamma}, \tag{3}$$

FIG. 1.—Density distribution in the plane of the gas disk, coded on a logarithmic scale, at time $t = 18.25$ for runs A, B, C, and D, which have different assumed levels of clumpiness. The MBHs are indicated in each plot by the black dots, and each MBH has 1% of the mass of the gas disk. The clumpiness is varied by varying the parameter K in eq. (3), as tabulated in Table 1, and the form of the resulting density distribution varies from relatively smooth spiral features for a large value of K (run D) to one with dense clumps and filaments for small K (run A).
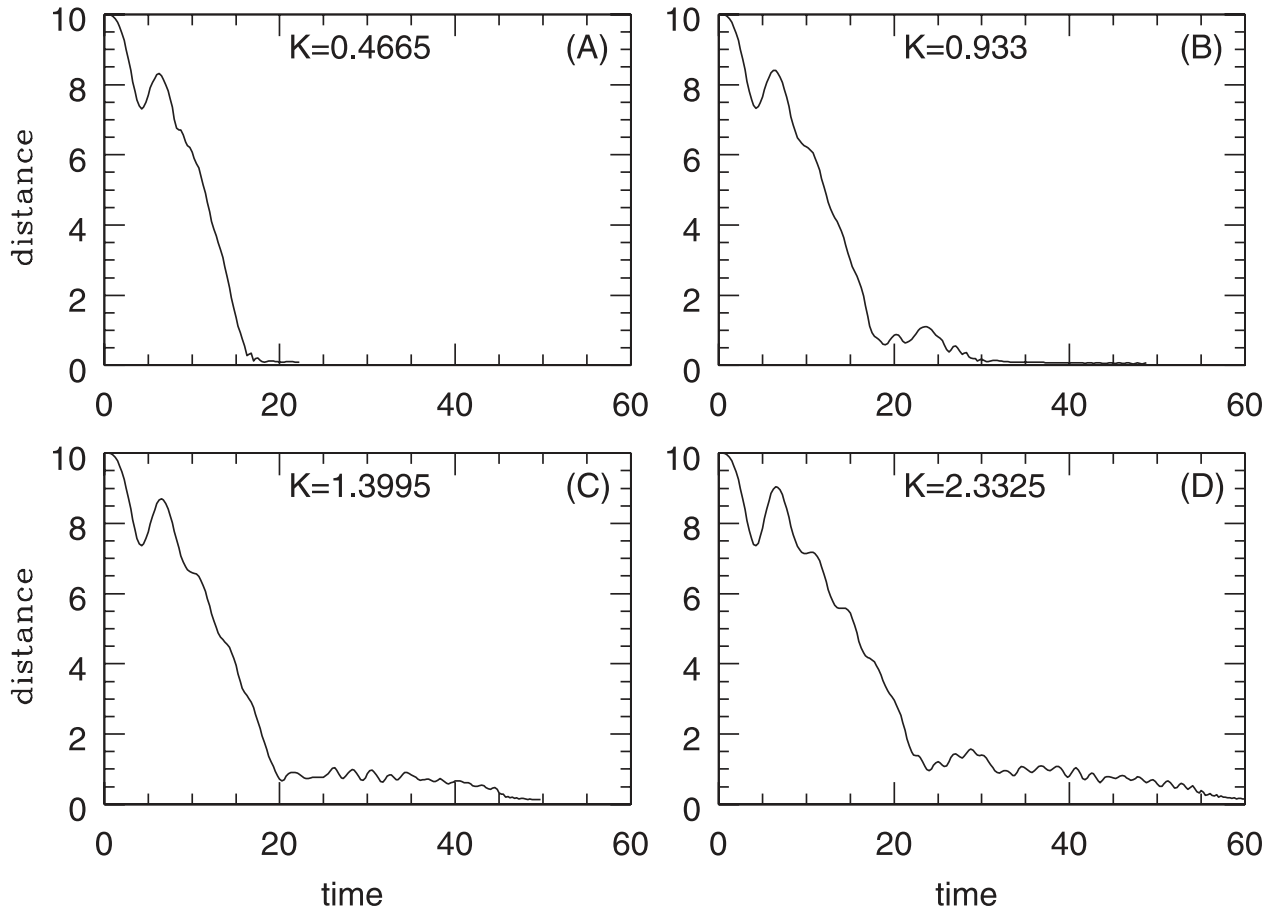
Fɪɢ. 2.—Evolution of the binary separation for runs A, B, C, and D with four different values of K, as indicated. In all cases the mass of each MBH is 1% of the mass of the gas, and the orbit of the binary is in the plane of the disk. A transition phase with a period of slower evolution after $t \sim 20$ becomes increasingly prominent as K is increased.

where γ is equal to 5/3 and K is a free parameter corresponding to the entropy of the gas. We vary K to simulate different mean gas properties and different degrees of clumpiness; smaller values of K yield a colder, thinner, and denser disk with greater clumpiness. We consider four different values for K, 0.4665, 0.933, 1.3995, and 2.3325, and we find that for these values, the disk thickness is 0.5, 0.625, 0.8, and 1, respectively, in our simulation units, while the fraction of the gas having densities higher than 10^5 cm^{-3} is 60%, 30%, 20%, and 10% when scaled to the properties of typical ULIRGs using the simulation units defined previously.

In the model that we just described, we introduce an MBH binary in a circular orbit, and we follow the subsequent dynamical evolution of the system. Each MBH is modeled by a non-accreting collisionless particle, with a gravitational softening length of 0.1, and the effects of gas accretion onto the MBHs will be studied in a subsequent paper. We evolve the system using the SPH code called GADGET (Springel et al. 2001). We are interested in studying the evolution of the MBH binary separation with different values of the model parameters. The first parameter considered is K, which controls the level of clumpiness and the mean gas properties. Second, since the total amount of gas in the nucleus of a merging system varies from one case to another, and since the black hole masses may also vary, we consider several different values for the mass ratio between the MBHs and the gaseous disk. Third, since the black holes need not orbit in the plane of the disk, we vary the inclination angle between the plane of the binary and the plane

of the disk. Table 1 lists the parameters used in the different simulations.

4. RESULTS

4.1. *Effects of Varying K*

We start by varying the constant K that controls the level of clumpiness and the mean gas properties. We consider four different values for K: 0.4665, 0.933, 1.3995, and 2.3325. To illustrate the effects, we consider first an MBH binary in which each black hole has a mass equal to 1% of the total gas mass, initially in a circular orbit with a binary separation of 10, or half of the disk diameter.

Figure 1 illustrates a representative stage in the evolution of the system for the four different values of K, showing the face-on density distribution in the gas disk at the same time in each case ($t = 18.25$). The density distribution varies from relatively smooth spiral features to dense clumps and filaments as we reduce the parameter K. For K values of 0.4665, 0.933, 1.3995, and 2.3325, the disk thickness is 0.5, 0.625, 0.8, and 1, respectively. In our model, the disk thickness is determined by the sound speed $c_S = \left[(5/3) K \rho^{2/3} \right]^{1/2}$ implied by the adiabatic equation of state used, and that ranges from 0.4 to 0.5 (or between 62 and 78 km s^{-1} if we rescale using the simulation units defined in § 3) for different values of K. In reality, the sound speed c_S corresponds to internal turbulent motions in the gas, which are observed to be of this order, as noted in § 2. Our aim is to represent the observed highly turbulent molecular disk
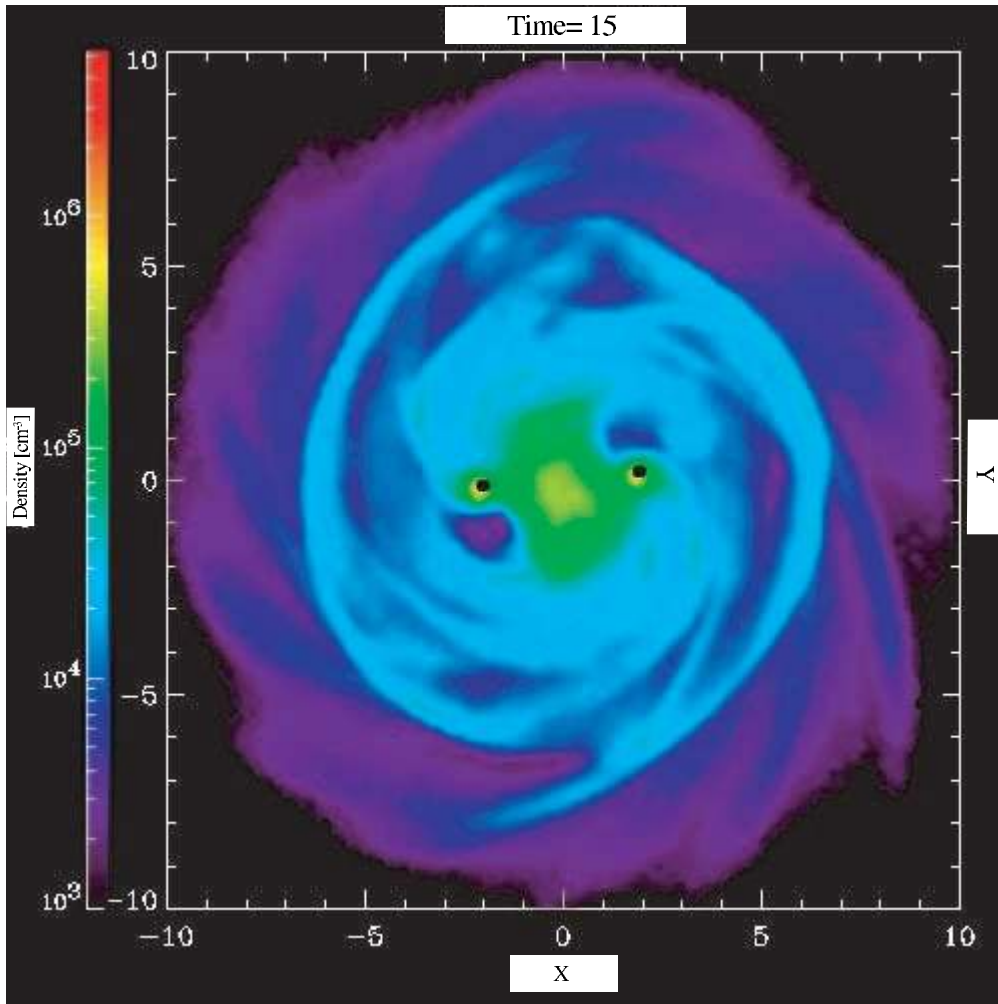
Fig. 3.—Density distribution in the plane of the gas disk for run C at time $t = 15$, showing in more detail the spiral shocks produced by each orbiting MBH. Qualitatively, as was found in Paper I, the response of the gas to the presence of the MBHs is a lagging density enhancement and a spiral shock that propagates outward from each MBH.

(DS98), in which a turbulent velocity dispersion of $\sim$100 km s^{-1} determines the disk thickness.

Figure 2 shows the evolution of the binary separation in these four cases over several orbits. In the early evolution of the system, the separation diminishes due to the dynamical friction exerted by the background medium; this regime lasts until the binary separation is approximately 1. Figure 3 shows the density distribution in the plane of the disk at $t = 15$ for run C. As found in Paper I, the response of the gaseous medium to the presence of the MBHs is a lagging density enhancement and a spiral shock that propagates outward from each MBH.

A notable feature of Figure 2 is the marked increase of the coalescence timescale when the binary separation is less than 1. In order to address the origin of this change, we compute the gravitational torques exerted by the surrounding material for run C. Figure 4a shows the evolution of the gravitational torques (in code units) exerted onto the MBH binary by the different background mediums: gaseous (*red line*), stellar (*green line*), and total (gaseous + stellar, *black line*). Figure 4b reproduces the evolution of the binary separation for run C (Fig. 2c). This figure clearly shows that the origin of the marked increase of the coalescence timescale at $t = 20$ is, as expected, due to a marked decrease of the gravitational torques from the gas component between $t = 18$ and 20. Figure 4a also shows that the

gravitational torques from the stellar component are, on average, one-third of the gravitational torques from the gas, and therefore the binary separation diminishes mainly due to dynamical friction exerted by the background gas.

By analyzing the evolution of the gravitational torques exerted onto the MBHs, we determine that the bulk of the torque on each MBH is generated in a region of radius $r = 1.1$ centered on each MBH. At any given time between $t = 0$ and 18 (before the marked decrease of the torques), these regions always generate at least 90% of the gravitational torques. Figure 5 shows the density distribution in the plane of the gas disk for run C, illustrated at four different times: 15, 18, 20, and 22.5. In this figure, the black circles centered on each MBH indicate $r = 1.1$. Figure 5 clearly shows that the marked decrease of the gravitational torques between $t = 18$ and 20 in Figure 4a coincides with when these circles overlap in Figure 5. The decrease of the gravitational torques happens because the region that produces the bulk of the torques on each MBH cannot be larger than the separation between the two MBHs. Therefore, this region must be truncated, and the torque decreased, as the MBHs approach each other. This transition regime corresponds to the intermediate stage between the dynamical friction and the ellipsoidal torque regimes discussed in Paper I.

The binary evolution has a strong dependence on the parameter K, and the cases with lower K suffer a stronger deceleration.
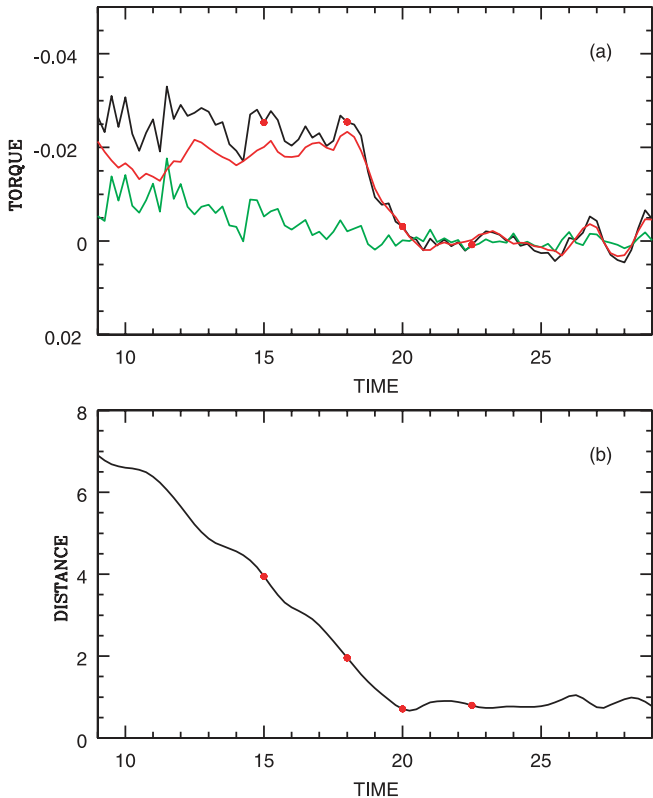
FIG. 4.—(a) Evolution of the gravitational torques (in code units) exerted onto the MBH binary. The red line represents the torque exerted by the gaseous background, the green line represents the contribution of the stellar background to the torque, and the black line is the sum of the gaseous and the stellar contributions. A negative torque means that angular momentum is extracted from the binary. (b) Evolution of the binary separation for run C; this is the same calculation shown in Fig. 2c. The comparison of (a) and (b) clearly shows that the origin of the marked increase of the coalescence timescale at $t = 20$ is, as expected, due to a marked decrease of the gravitational torques from the gas component between $t = 18$ and 20.

The explanation involves the gas density close to each MBH, which is higher for lower K. As a result, because the dynamical friction exerted by the background gas is stronger in a denser environment, the binary MBH separation shrinks faster in the cases with lower K. The effect of K on the local density is illustrated in Figure 6, which shows the average gas density within $r = 0.5$ around each MBH as a function of time for the four different values of K. The figure shows that the density in the vicinity of each MBH varies strongly between the different cases, and this produces important differences in coalescence timescale, as seen in Figure 2. In run A, the drastic increase in density seen in Figure 6 compensates for the decrease in the efficiency of the dynamical friction exerted by the background gas in the transition period, thereby keeping the coalescence timescale roughly constant. However, as we increase K (respectively in runs B, C, and D), the increase of density is less, making the increase in coalescence timescale more obvious. In the isothermal sphere model of Paper I, the gas becomes increasingly concentrated around the central MBH binary, qualitatively as in run A, and as a result there is no distinct transition period.

In § 5, we show that in the later stages, the subsequent evolution of the binary leads to rapid coalescence in less than another 5 time units. Therefore, the binary spends most of its time in the stages of evolution discussed above, making it important to understand the changes in coalescence timescale under different values of the model parameters.

4.2. Effects of Varying the Orbital Inclination Angle

Our second parameter is the inclination angle between the plane of the disk and the plane of the binary. We perform simulations with four different inclination angles: $0°$, $22°.5$, $45°$, and $67°.5$. As in § 4.1, we consider an MBH binary initially in a circular orbit with an MBH mass equal to 1% of the total gaseous mass, and for these runs we adopt an equation of state with $K = 0.933$, as in run B.

Figure 7 shows the evolution of the binary separation in these four cases over several orbits. Although the case with $i = 22°.5$ has a coalescence timescale similar to the coplanar case, for inclination angles of $45°$ and $67°.5$ the coalescence timescales are increased by factors of 3 and 4, respectively. The reason for this difference is that in these cases, the early evolution of the binary is driven by the dynamical friction exerted by the stellar bulge instead of by the dynamical friction of the gas disk. Figure 8 shows a comparison of the evolution of the binary separation for the case with $i = 45°$ (black curve) with the evolution of the binary in the same bulge but without the gaseous disk (green curve). The agreement between these curves shows that the binary coalescence is driven up to time $t = 50$ by the dynamical friction exerted by the stellar bulge. In all cases, the drag due to the gas disk eventually becomes dominant after the separation becomes small enough that the MBH binary spends more than 50% of its time in the disk, and the evolution thereafter proceeds much as in the coplanar case.

4.3. Effects of Varying the Black Hole to Gas Mass Ratio

Finally, we study the effect of varying the ratio between the mass of the MBHs and the mass of the gas disk. We consider four cases with black hole masses of 1%, 3%, 5%, and 10% of the total gas mass. We introduce an MBH binary initially in a circular orbit in the plane of the disk, using an adiabatic equation of state with $K = 0.933$.

Figure 9 shows the evolution of the binary separation in these four cases over several orbits. In the early evolution of the system, when the separation diminishes due to the dynamical friction exerted by the background medium, the binary coalescence timescale depends on the black hole mass, with the more massive cases suffering a stronger deceleration. The time required for the binary separation to decrease by 75% varies from $t \sim 16$ for $M_{BH} = 0.01 M_{gas}$ to $t \sim 8$ for $M_{BH} = 0.1 M_{gas}$. In units of the initial orbital period, this time varies from 2 to 1 orbital periods. The trend is similar to that obtained in Paper I for a smooth gaseous medium and is qualitatively consistent with the Chandrasekhar formula.

The dependence of the binary coalescence timescale on the black hole mass changes when the binary separation arrives in the transition regime discussed in § 4.1. Figure 9 shows that at later times there is no longer a clear dependence on the black hole mass; this is because as we increase the black hole mass, the wake formed is stronger, but the truncation of the wake by the gravity of the other MBH is also stronger, weakening the strong correlation with black hole mass. In fact, for the case of $M_{BH} = 0.1 M_{gas}$, we see a small increase in the coalesce timescale in the transition regime. In this case, the disk is starting to be globally perturbed by the presence of the MBHs, as seen in Figure 10, and not only locally, as before. Tidal and/or resonant forces are starting to evacuate gas from the central region, and these effects become more important as we continue increasing the black hole mass. As a result, in the overall evolution of the binary separation, the dependence on the black hole mass is only weak, mainly because there is not a clear dependence on mass during the later times.
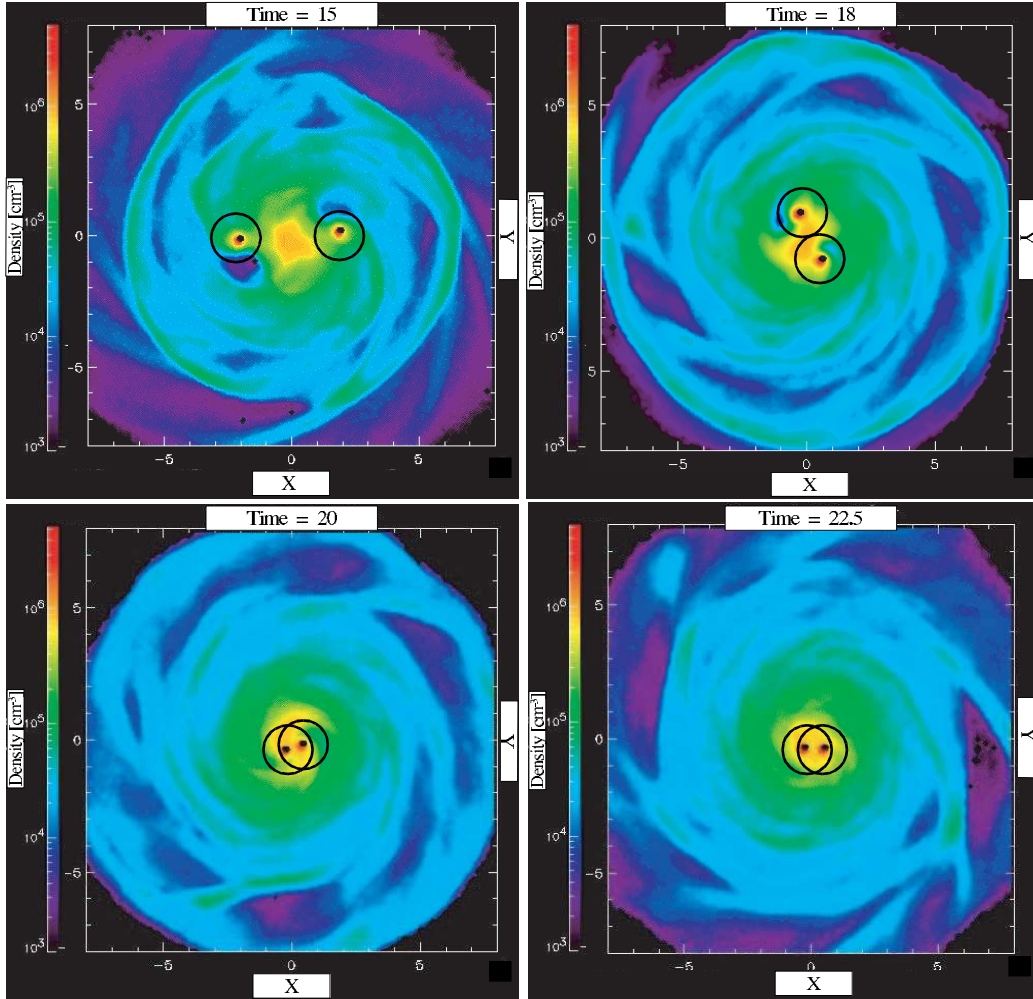
Fig. 5.—Density distribution in the plane of the gas disk for run C, illustrated at four different times, 15, 18, 20, and 22.5, which are indicated by the red dots in Figs. 4*a* and 4*b*. When the regions that generate more than 90% of the torques (*black circles*) merge between $t = 18$ and 20, the region that produces the bulk of the torques on each MBH is truncated, and therefore the torque decreases. This is responsible for the marked decrease of the gravitational torques between $t = 18$ and 20 in Fig. 4*a*.

In order to determine when the gas becomes no longer important in driving the coalescence of the binary, we continue increasing the black hole mass. We consider two more cases with black hole masses of 30% and 50% of the total gas mass. Figure 11 shows the evolution of the binary separation in these two cases over several orbits. We found that the coalescence tends to stall in the case in which the black hole mass equals 50% of the total mass (Fig. 11, *black line*). This happens because strong tidal and/or resonant forces create a circumbinary gap, as seen in Figure 12, and therefore the gravitational drag is no longer effective. The interaction of a binary with a circumbinary disk in cases where the total gas mass is typically equal to or smaller than the binary mass has been widely studied in the context of star/planetary formation (Lin & Papaloizou 1979; Goldreich & Tremaine 1982; Artymowicz & Lubow 1994, 1996; Armitage & Natarajan 2002), where a similar circumbinary gap is found. The criterion for opening a gap is discussed in § 6.

5. FINAL EVOLUTION USING HIGHER RESOLUTION SIMULATIONS

The runs described above were continued until the MBH separation approached the assumed gravitational softening length of 0.1, at which point the evolution of the system artificially stalls. To continue the evolution of the binary, it is necessary to reduce the gravitational softening length, something that is extremely expensive computationally. We choose to reduce it from $\epsilon_{soft} = 0.1$ to 0.0025 in order to follow the evolution of the binary separation by one more order of magnitude, and we apply this procedure to the cases where each MBH has 1% of the total mass in gas and the binary is in the plane of the disk, again for the four runs with different values of K. We reduce the softening length when the binary separation is approximately 0.75, which occurs at different times for different values of K.

Figure 13 shows the evolution of the binary separation in these four cases over several orbits. The black curves are the same calculations shown in Figure 2, but on a logarithmic scale, and the red curves show the results for the simulations with a smaller softening length.

In the early evolution of the system, the black and red curves show almost the same behavior in each case. The situation changes drastically when the binary separation becomes less than about 0.25, that is, when the binary arrives at separations comparable to the "gravitational influence" radius of the black hole: $R_{inf} = 2GM_{BH}/(v_{BH}^2 + c_S^2)$. For example, at time 16 in run A, in which the black hole mass M_{BH} is 0.01, the MBH velocity v_{BH} is 1.1, and the sound speed c_S is $(5P/3\rho)^{1/2} = 1.01$ in the vicinity (within $r = 0.1$) of each MBH, the gravitational influence radius R_{inf} is 0.2. At these distances, the binary completely
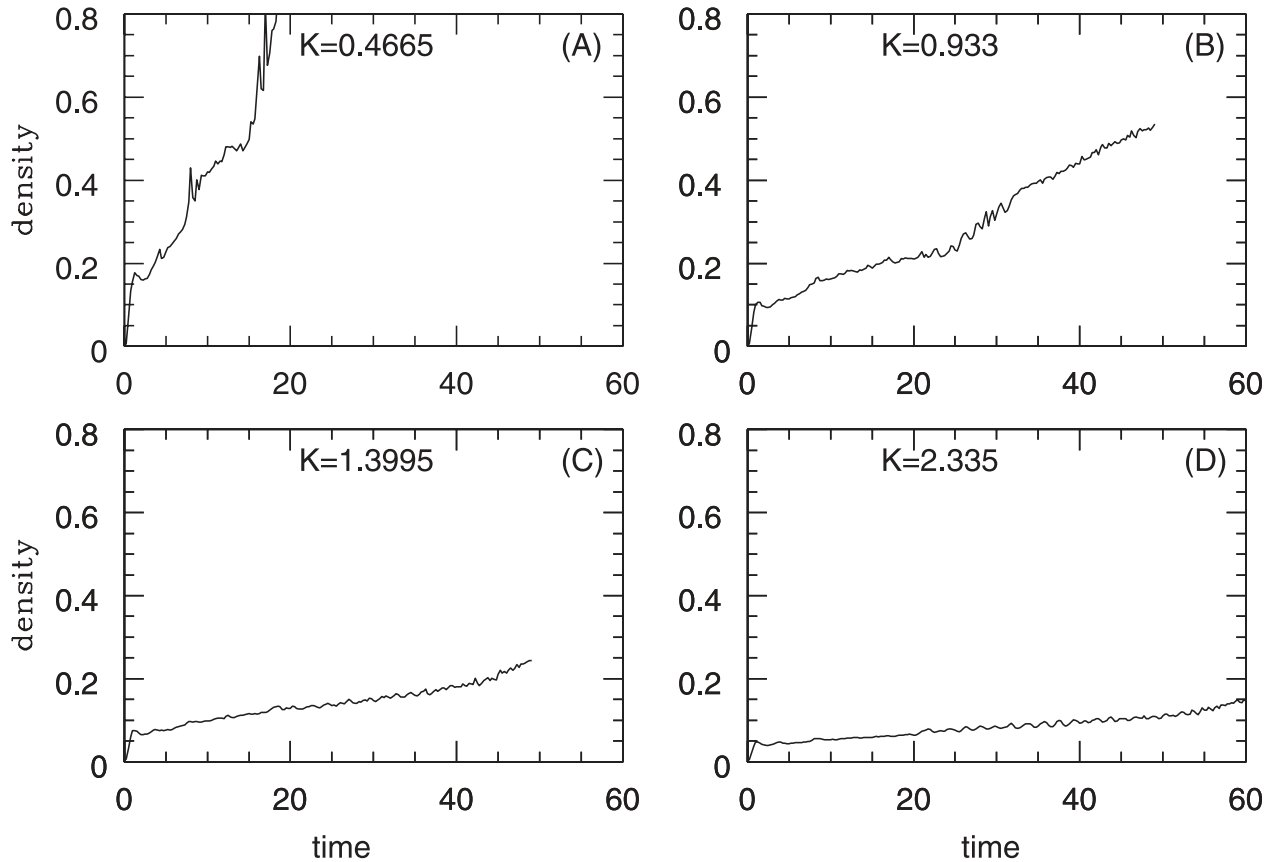
FIG. 6.—Average density within $r = 0.5$ around each MBH as a function of time for four different values of K: 0.4665, 0.933, 1.3995, and 2.3325. The density in the vicinity of each MBH increases strongly as K decreases, accounting for the faster evolution shown in Fig. 2 for smaller values of K. For all of these runs, $M_{BH} = 0.01 M_{gas}$ and $i = 0°$.
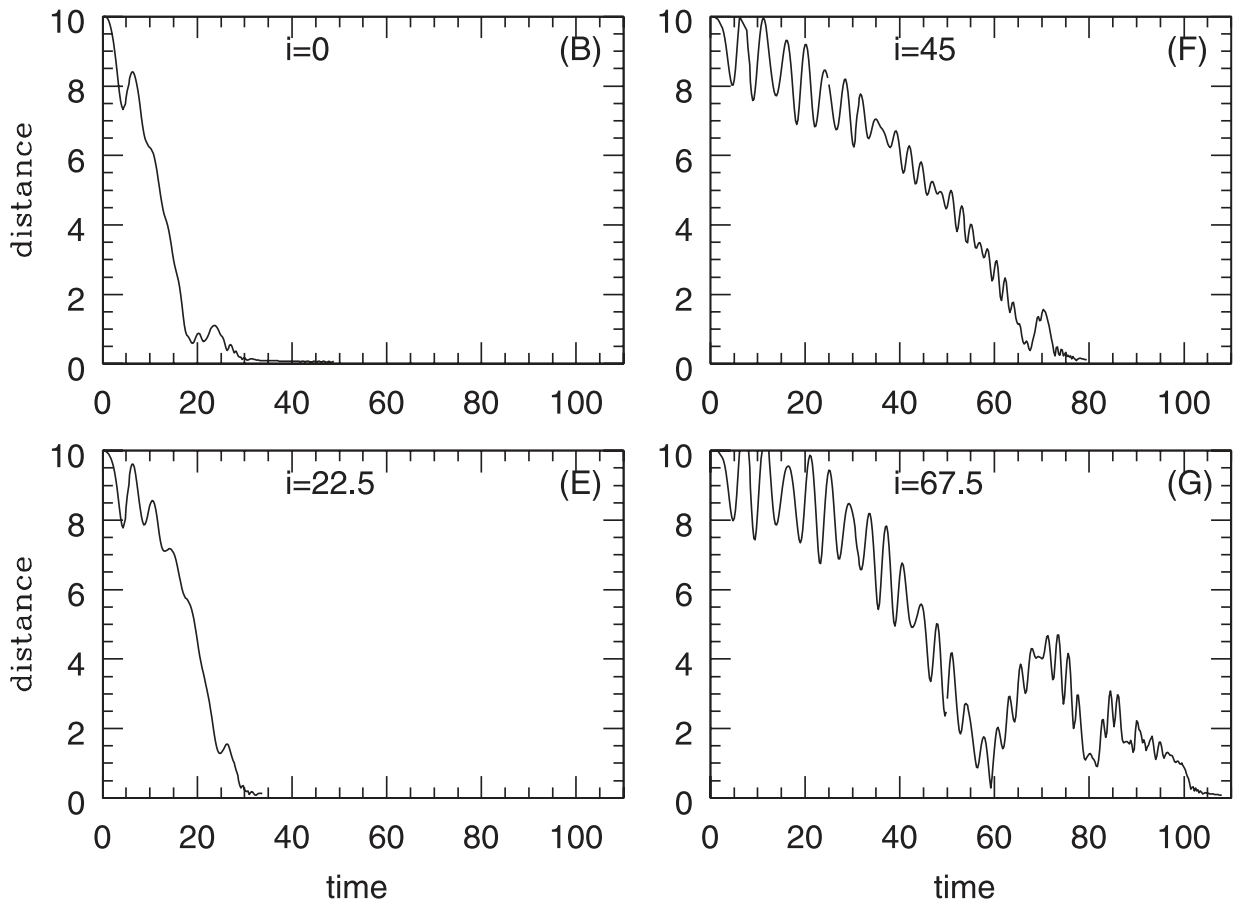

FIG. 7.—Evolution of the binary separation for runs B, E, F, and G with inclination angles of $0°$, $22°.5$, $45°$, and $67°.5$, respectively, between the plane of the disk and the plane of the binary. For all of these runs we adopt an equation of state with $K = 0.933$, and the mass of each MBH is 1% of the mass of the gas.
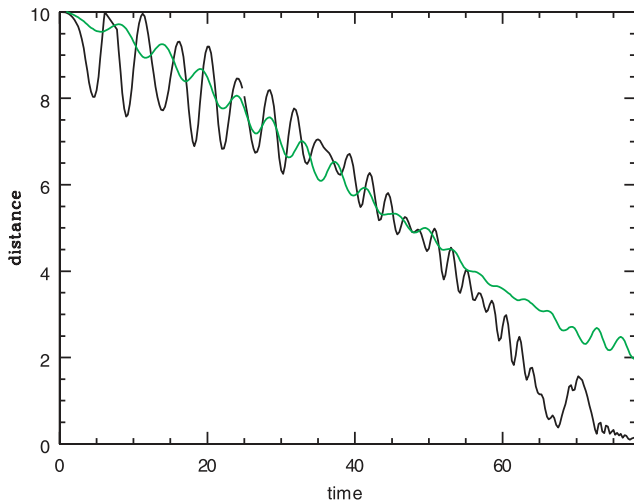
FIG. 8.—Evolution of the binary separation for the case in which the inclination angle between the plane of the disk and the plane of the binary is 45°. The black curve shows an enlargement of the curve shown for run F in Fig. 7, and the green curve shows the result of a run assuming the same stellar bulge but no gas disk. For these runs, $K = 0.933$ and $M_{BH} = 0.01M_{gas}$.

ranges from 0.225 to 0.3 in these four cases. Therefore, the transition to the new regime is only weakly dependent on K.

Figure 14 shows the density enhancement produced by the MBHs in the gaseous medium for the simulation with $K = 1.3995$ at four different times: 43.2, 44, 44.8, and 45.6. Figure 14 clearly shows that the rapid decay in the binary separation, which starts at around $t = 44.8$, coincides with the formation of the ellipsoid. In this figure, the black circles centered on each MBH indicate the gravitational influence radius R_{inf}, and the figure shows that the trailing ellipsoid forms when these circles overlap. The axis of the ellipsoid is not coincident with the binary axis, but lags behind it, and this offset produces a gravitational torque on the binary that is now responsible for the angular momentum loss. This ellipsoidal torque mechanism was extensively studied in Paper I and is able to reduce the binary separation to distances where gravitational radiation is efficient.

In the simulations described above, we reduced the gravitational softening length, but we maintained the number of SPH particles used. In order to verify that we have enough resolution to resolve adequately the region inside $r = 1$, where the dynamics of the final coalescence occurs, we repeat one of these simulations while increasing the number of particles. We use the particle splitting procedure described in Paper I to achieve this goal. The procedure is applied to the case where $K = 1.3995$. We split the SPH particles at a time of 40 when the binary enters the $r < 0.75$ region; for each parent particle we introduce $N_{split} = 8$ child particles, and therefore we increase the number of particles to 1,882,648.

dominates the gravitational potential in its vicinity, and the response of the medium to that gravitational field is a trailing ellipsoidal density enhancement, as was found in Paper I. The formation of the ellipsoidal density enhancement typically occurs when the binary separation is about $1.5R_{inf}$, and that value
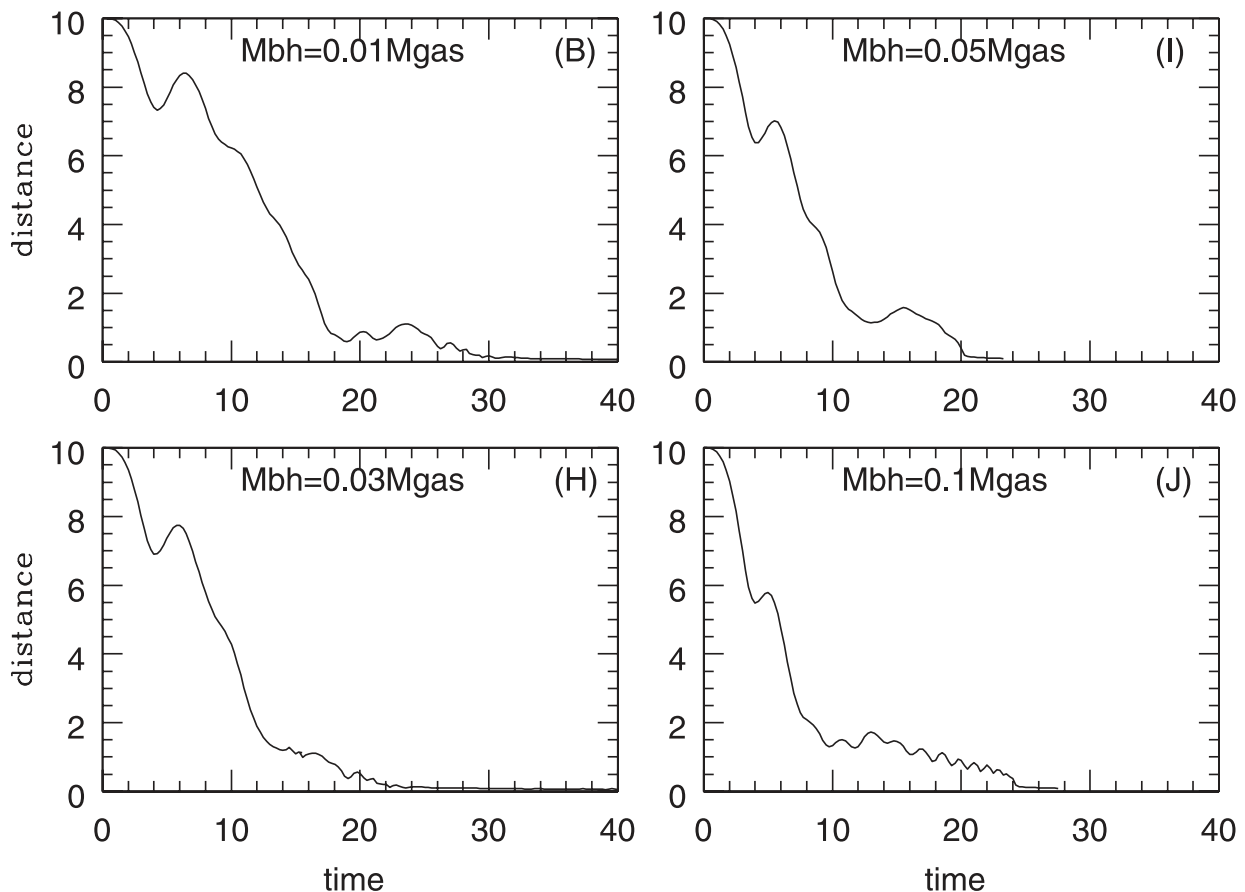

FIG. 9.—Evolution of the binary separation for runs B, H, I, and J, which assume four different ratios between the mass of each MBH and the mass of the gas disk: 0.01, 0.03, 0.05, and 0.1, respectively. For these runs, we adopt an equation of state with $K = 0.933$, and the orbit of the binary is in the plane of the disk. Overall, there is only a weak dependence of the resulting coalescence time on the mass of the MBHs, owing mainly to the weak or even inverse dependence during the later stages.
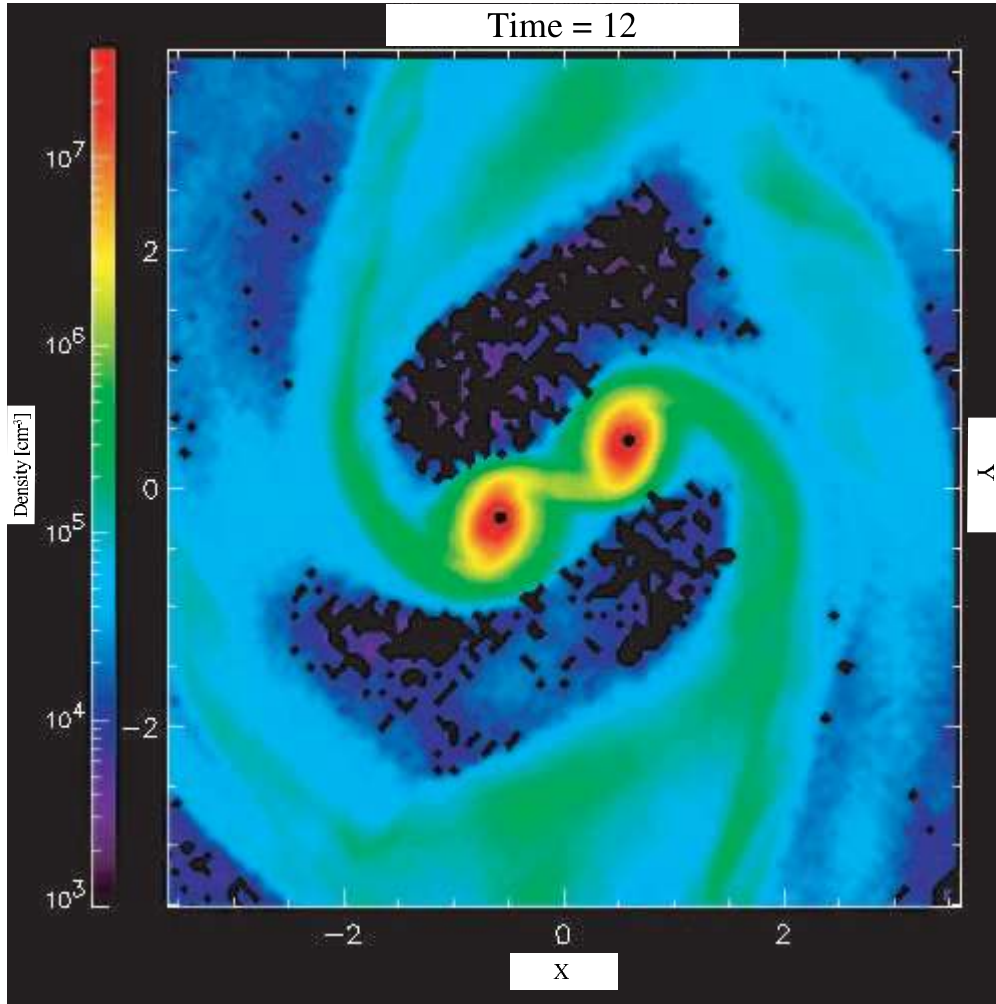
FIG. 10.—Density distribution in the plane of the disk for run J at $t = 12$. The black dots indicate the positions of the MBHs, and in this simulation the mass of each MBH is equal to 10% of the mass of the gas. The gas disk is globally perturbed and forms transitory gaps, as a response to the presence of the MBHs.
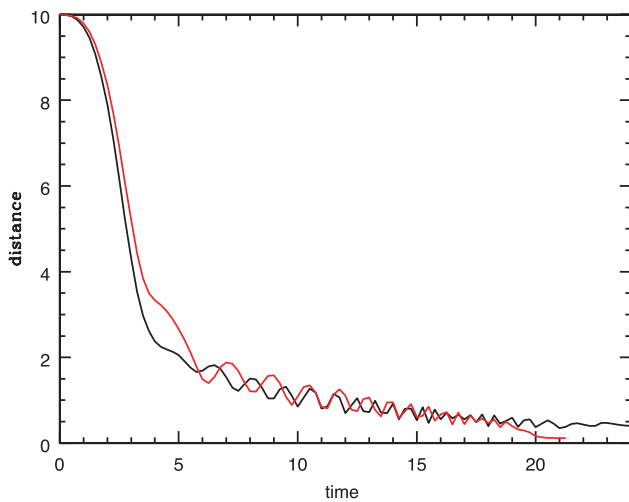

FIG. 11.—Evolution of the binary separation for runs K and L, which assume relatively large MBH masses. The black curve shows the evolution of the binary when $M_{BH} = 0.5M_{gas}$, and the red curve shows the calculation with $M_{BH} = 0.3M_{gas}$. For these runs, we adopt an equation of state with $K = 0.933$, and the binary's orbit is in the plane of the disk. The evolution of the run with $M_{BH} = 0.5M_{gas}$ almost stalls at late times because of the clearing of a gap in the disk, as illustrated in Fig. 10.

Figure 15 shows the evolution of the binary separation for the high-resolution calculation. The red curve is the same calculation shown in Figure 13, and the green curve shows the MBHs' separation in the high-resolution calculation. The result is qualitatively the same and quantitatively very similar to the low-resolution calculation. This supports the validity of the results shown by the red curves in Figure 13, based on the low-resolution calculations.

Finally, our model can be scaled to physical units by using the simulation units defined in § 3: [mass] $= 5 \times 10^9 \, M_\odot$, [time] $= 2.5 \times 10^5$ yr, [velocity] $= 156.46$ km s^{-1}, and [distance] $= 40$ pc. In these units, which represent the physical conditions in the inner regions of an ULIRG, the coalescence timescale varies between 5×10^6 and 2.5×10^7 yr in all of the cases considered. During the ellipsoidal torque regime, the binary reaches a final separation of 0.1 pc (our resolution limit) in only $\sim 10^6$ yr for these typical ULIRG parameters.

5.1. Gravitational Radiation

The final phase in the evolution of a binary MBH occurs when eventually the MBHs become close enough to allow gravitational radiation to become an efficient mechanism for angular momentum loss.
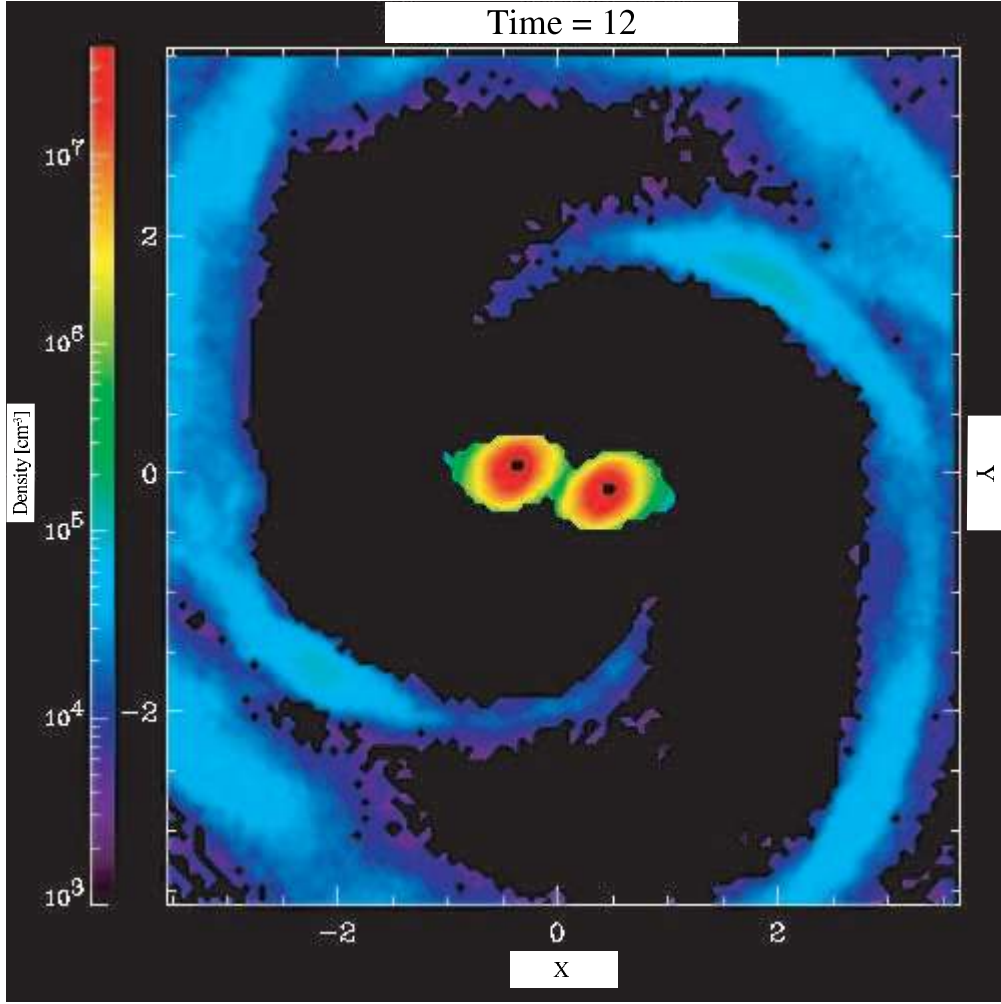
Fig. 12.—Density distribution in the plane of the disk for run L at $t = 12$. The black dots indicate the positions of the MBHs, and in this simulation the mass of the binary is equal to the mass of the gas. The gas response to the presence of the MBHs is a circumbinary gap created by the strong tidal and/or resonant forces near the MBHs.

For an equal-mass binary and scaled to convenient units, the gravitational radiation timescale (Peters 1964; see eq. [16] in Paper I) is

$$t_{gr} = 2.9 \times 10^6 \text{ yr} \left(\frac{a}{0.01 \text{ pc}}\right)^4 \left(\frac{10^8 \, M_\odot}{M_{BH}}\right)^3 F(e), \quad (4)$$

where a is the binary separation, M_{BH} is the mass of each black hole, and $F(e)$ (see Paper I) contains the eccentricity dependence, which is weak for small e; e.g., $F(0) = 1$ and $F(0.5) \sim 0.205$. For a binary in which the mass of each MBH is $5 \times 10^7 \, M_\odot$ (corresponding in our simulations to the case where each MBH has 1% of the total mass in gas) and that has a separation of 0.01 pc, the gravitational radiation coalescence timescale is $t_{gr} = 1.16 \times 10^7$ yr. If we extrapolate our results to separations of 0.01 pc (at the end of our simulations the final separation is 0.1 pc), we predict that the MBH binary will merge in $\sim 10^7$ yr for all values of K. We feel confident that we can extrapolate our results to smaller separations because the ellipsoidal torque model studied in Paper I describes successfully the late evolution of the binary MBH, and it predicts that the separation should reach 0.01 pc within less than another 10^6 yr.

6. GAP-OPENING CRITERIA

As we found in § 4.3, when the MBH binary is able to open a circumbinary gap in the disk, the gas no longer plays an im-

portant role in the coalescence of the binary; the problem then reduces to the evolution of a black hole binary at the center of a stellar system, which has been extensively studied in the literature (Begelman et al. 1980; Makino & Ebisuzaki 1996; Quinlan 1996; Milosavljevic & Merritt 2001, 2003). Therefore, it is important to determine the critical MBH mass needed to open the gap.

The criterion for opening a gap can be determined by comparing the gap-closing and gap-opening times (Goldreich & Tremaine 1982). The angular momentum ΔL that must be added to the gas to open a gap of radius Δr in a disk with thickness h is $\Delta L \approx \rho(\Delta r)^2 hrv$. Using the dynamical friction formula (Chandrasekhar 1943; Ostriker 1999), we infer that the torque that each black hole exerts on the disk is

$$T \approx 4\pi\rho r \left(\frac{GM_{BH}}{v_{BH}}\right)^2 f^{(star, gas)}(\mathcal{M}), \quad (5)$$

where $\mathcal{M} = v_{BH}/c_S$ and $f^{(star, gas)}$ is a dimensionless factor that depends on the nature, stellar or gaseous, of the background medium (see eqs. [7]–[10] in Paper I). This torque will supply angular momentum ΔL in a time $\Delta t_{open} = \Delta L/T$. The tendency of for gap formation is opposed by turbulent diffusion, which fills up a gap of width Δr on a timescale $\Delta t_{close} = \Delta r/v_{turb}$; as mentioned before, in our adiabatic model the turbulent velocity dispersion is represented by the sound speed ($c_S = v_{turb}$). Gap formation occurs if $\Delta t_{close} \gtrsim \Delta t_{open}$, and taking into account
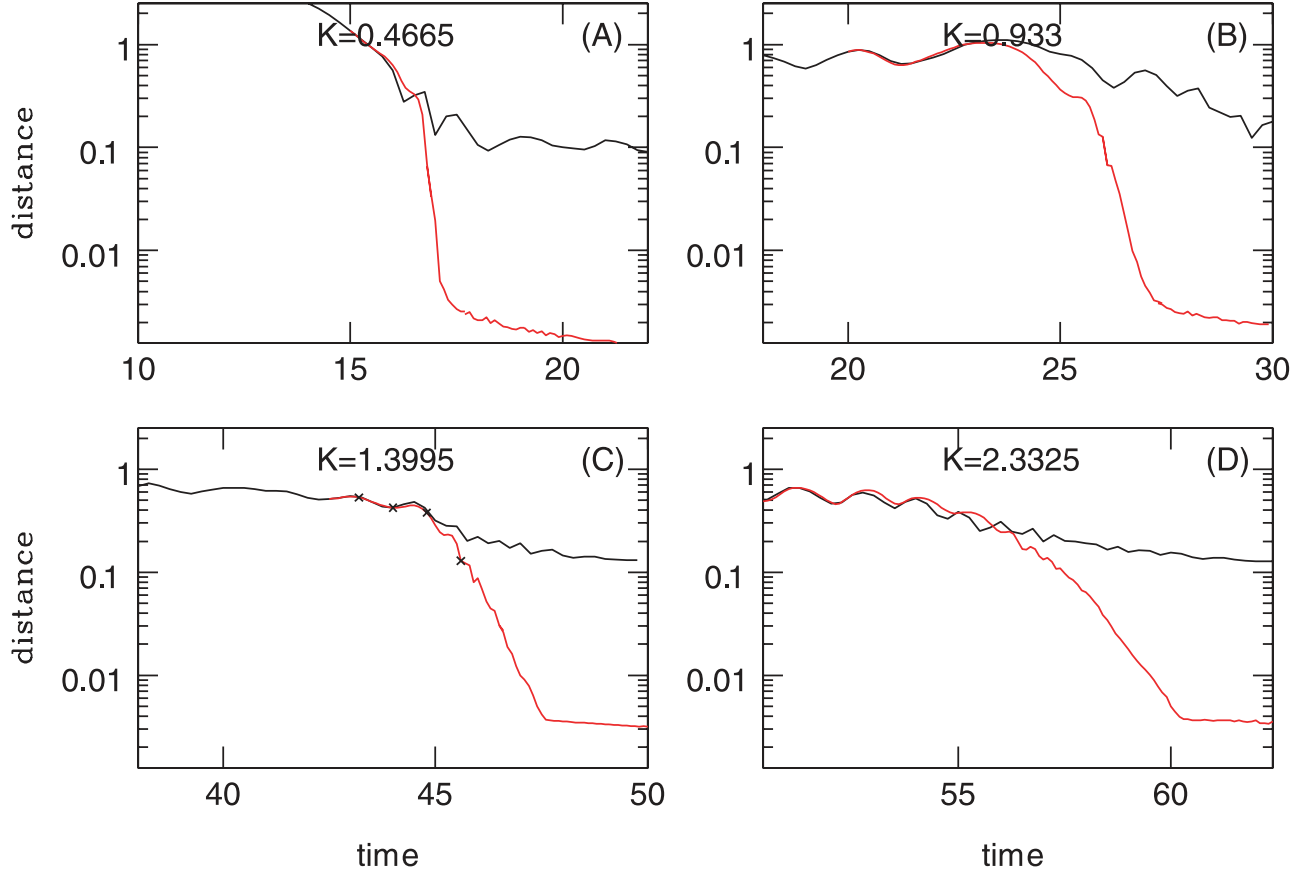
FIG. 13.—Final evolution of the binary separation for runs A, B, C, and D with four different values of K. In all cases the mass of each MBH is 1% of the mass of the gas, and the orbit of the binary is in the plane of the disk. The black curves are the same calculations shown in Fig. 2, but on a logarithmic scale. The red curves show the results for the simulations with a smaller softening length. The black crosses in run C correspond to the four different panels in Fig. 14.

that $v_{BH} = [GM(r)/r]^{1/2}$, where $M(r)$ is the total enclosed mass at radius r, this criterion can be written

$$M_{BH} \gtrsim \sqrt{\frac{\alpha}{4\pi f(\mathcal{M})\mathcal{M}}} \left(\frac{h}{r}\right) M(r), \qquad (6)$$

where α is the ratio of gap radius to disk thickness, defined by $\Delta r = \alpha h$. The simulation with black hole masses equal to 50% of the total gas mass suggests that a stable circumbinary gap forms when the MBHs are at a radius $r \sim h$, with a gap width of $\Delta r \sim 3h$ ($\alpha = 3$). For the parameters used in our simulation, equation (6) corresponds to the condition $M_{BH} \geq 0.46 = 0.46 M_{gas}$, in agreement with our result of § 4.3 (Fig. 12) that a circumbinary gap opens when $M_{BH} = 0.5 M_{gas}$.

As seen in equation (6), the critical mass at a given radius depends on the total enclosed mass. Because approximately 80% of the dynamical mass in the region of interest is contributed by the stellar bulge (DS98), we assume that $M(r) = G^{-1}r\sigma_c^2$, where σ_c is the central stellar velocity dispersion. The mass of the central black holes in nearby galaxies is observed to be correlated with the central velocity dispersion, measured within the central kiloparsec, by the so-called m-σ_c relation (Tremaine et al. 2002; Merritt & Ferrarese 2002),

$$M_{binary} = 2M_{BH} = \left(\frac{\sigma_c}{200 \text{ km s}^{-1}}\right)^4 10^8 \ M_\odot, \qquad (7)$$

where we assume that the mass of the binary correlates in the same way with the central velocity dispersion of the merged

bulges. Using this relation, equation (6) can be written in a simpler form,

$$M_{BH} \gtrsim \frac{\alpha}{4\pi f(\mathcal{M})\mathcal{M}} \left(\frac{h}{pc}\right)^2 1.74 \times 10^6 \ M_\odot. \qquad (8)$$

As mentioned earlier, our result of § 4.3 (Fig. 12) suggests that a stable circumbinary gap forms when $\Delta r \sim 3h$, and therefore we set $\alpha = 3$. For a Mach number of the order of unity, the critical mass required for a gap to form then reduces to

$$M_{BH} \gtrsim \left(\frac{h}{pc}\right)^2 7.2 \times 10^5 \ M_\odot. \qquad (9)$$

For typical ULIRGs (DS98), h is at least of the order of 40 pc. Therefore, the formation of a circumbinary gap will be prevented, since the observed MBH masses range from 10^6 to a few times $10^9 \ M_\odot$ and thus are smaller than the critical mass required to open a gap, as given by equation (9). The formation of a circumbinary gap will be prevented, and the MBH binary will therefore coalesce as long as the disk thickness remains of the order of tens of parsecs. Observations show that even in nuclear molecular disks of mass $\sim 10^8 \ M_\odot$ the velocity dispersions are still ~ 40 km s^{-1}, indicating that disk thicknesses of the order of tens of parsecs are present, and this result is independent of whether or not the galaxy hosts a starburst (Jogee et al. 2005). Thus, gas should play a dominant role in driving the mergers of black holes as long as the amount of gas present in the central kiloparsec is equal to or larger than this. In most
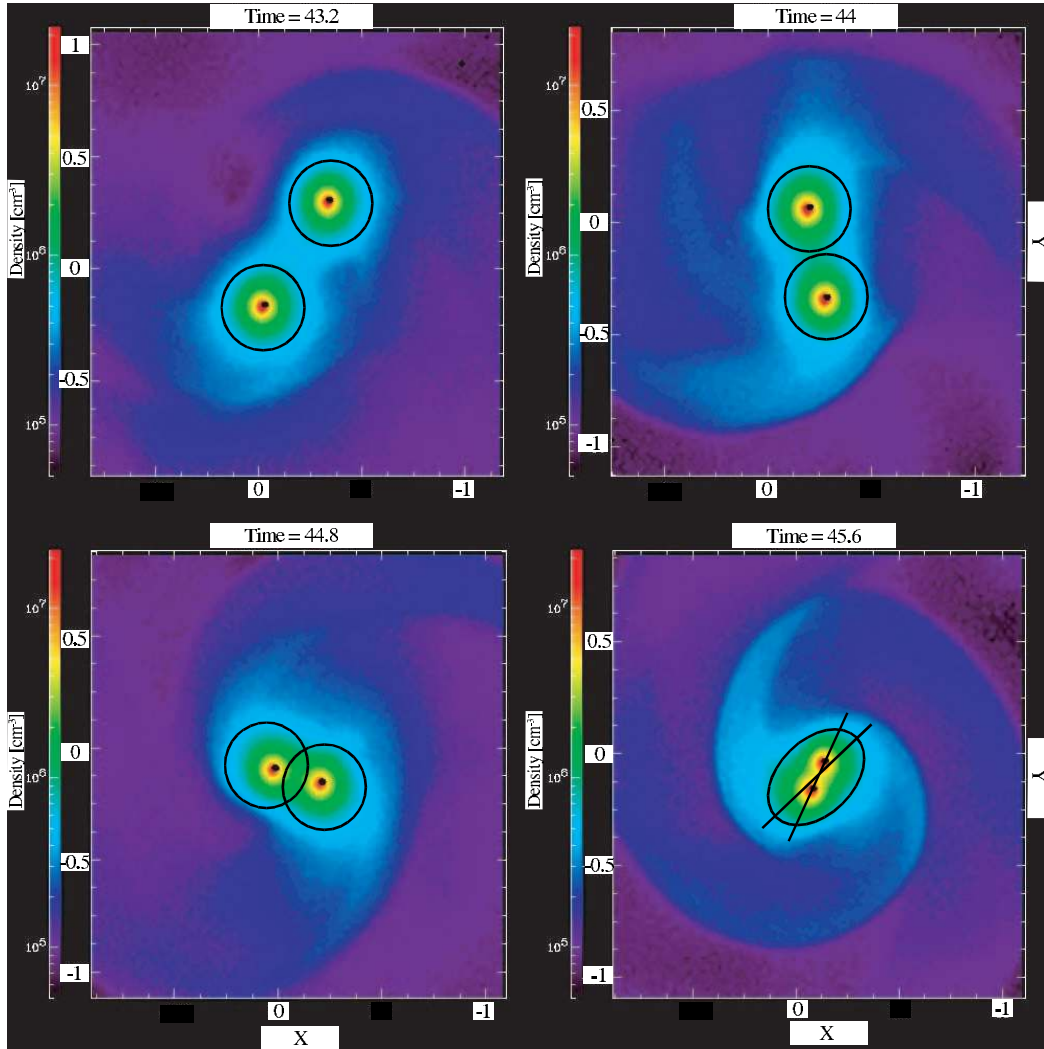
FIG. 14.—Density distribution in the plane of the gas disk for run C, illustrated at four different times, 43.2, 44, 44.8, and 45.6, which are indicated by crosses in Fig. 13c. When the regions within the gravitational influence radius of each MBH (*black circles*) merge at around $t = 44.8$, the gas forms a trailing ellipsoidal density enhancement bound to the binary that is responsible for the rapid decay in the binary separation at late times seen in Fig. 13.
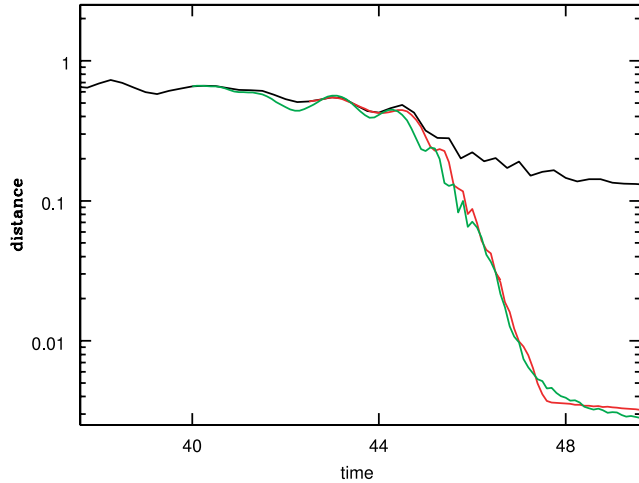
FIG. 15.—Final evolution of the binary separation for the case in which $K =$ 1.3995 (run C). The black curve is the same calculation shown in Fig. 2, but on a logarithmic scale. The red curve shows the result for the simulation with a smaller softening length, the same calculation shown in Fig. 13c. The green curve shows the MBHs' separation in the calculation that has both a smaller softening length and a much higher numerical resolution ($N_{SPH} = 1,882,648$). The result is qualitatively the same and quantitatively very similar to the low-resolution calculation. This supports the validity of the results shown by the red curves in Fig. 13, based on the low-resolution calculations. For these runs, $M_{BH} = 0.01 M_{gas}$ and $i = 0°$.

galaxy mergers a nuclear disk of at least this mass is expected, because a disk mass of the order of $10^8 M_{\odot}$ corresponds, for an average spiral galaxy like the Milky Way, to only 0.1% of the total mass being in gas, a small gas mass fraction compared to the 1%–50% present in Sa to Scd galaxies (Young et al. 1995). Taking into account that in a galaxy merger typically 60% of the gas originally present in the merging galaxies ends up in a massive nuclear disk, and allowing for some gas depletion due to star formation, we can conservatively conclude that in a merger of galaxies with at least 1% of their total mass in gas, a nuclear disk with mass $\geq 10^8 M_{\odot}$ will be present, and that the gas will then play a major role in the evolution and final coalescence of the binary.

On the other hand, if the masses of the black holes are greater by an order of magnitude or more than is expected from the m-σ_c relation, it is more probable that the MBH binary will form a circumbinary gap inside the central 100 pc of the disk. In this case, the feeding of gas into the MBHs and therefore their growth will almost be stopped. This suppresses an important accretion phase for MBHs, in which a nonnegligible part of the MBH mass is expected to be assembled, because without the gap, the accretion is predicted to be at a super-Eddington rate (Dopita 1997). However, the bulge will continue accreting gas and growing, especially in the central kiloparsec, where σ_c is measured, and therefore the stellar velocity dispersion will also continue growing and trying to reach the m-σ_c relation. Thus, gap formation can act as a self-regulatory mechanism for MBH growth, and this might play a role in helping to account for the origin of the m-σ_c relation.

7. CONCLUSIONS

In our previous paper (Paper I) we studied the role of gas in driving the evolution of a binary MBH, and we followed its evolution through many orbits and close to the point at which gravitational radiation becomes important. In Paper I, we presented results for a relatively idealized case in which the gas was assumed to be in a nearly spherical and relatively smooth

distribution, and we found important differences in the evolution of a binary MBH in a gaseous medium compared to a stellar background. In particular, we did not find any sign of ejection of the surrounding gas, as happens with stars in the later stages in the evolution of a binary MBH in a stellar system.

In the present paper, we have extended this work by studying more realistic models in which the gas is in a disk with the observed properties. We do not attempt a fully realistic description of the gas in merging galaxies, which often exhibits starburst activity, but adopt a simple polytropic equation of state with a variable coefficient K that allows us to represent gas with a varying degree of clumpiness. In this way we are able to represent gas with the observed range of densities in merging systems. We also vary the inclination angle between the plane of the binary and the plane of the disk and the mass ratio between the MBHs and the gaseous disk.

In the early evolution of the system, as in Paper I, the separation diminishes mainly due to the dynamical friction exerted by the background gaseous medium. We find a new transition regime that was not apparent in Paper I, when the region that produces the bulk of the torques is truncated as the MBHs approach each other. In this transition regime the dynamical friction from the gas is less effective, and therefore the coalescence timescale increases.

In the variety of simulations that we perform, we find that varying the parameter K, or the inclination angle between the plane of the binary and the plane of the disk, changes the binary coalescence timescale by less than a factor of 3. We also find that the dependence on the mass ratio between the MBHs and the gaseous disk is only weak, mainly because there is not a clear mass dependence in the transition regime. In all of the cases considered, the coalescence timescale varies between 2.5 and 12 initial orbital periods, or between 5×10^6 and 2.5×10^7 yr for typical ULIRGs.

The final evolution of the binary, when the binary MBH dominates the gravitational potential in its vicinity, is driven by the same trailing ellipsoidal density enhancement that was found in Paper I. The axis of the ellipsoid lags behind the binary axis, and this offset produces a gravitational torque on the binary that is now responsible for the continuing loss of angular momentum. The formation of the ellipsoidal density enhancement typically occurs when the binary separation becomes comparable to the gravitational influence radius of the black hole, $R_{inf} = 2GM_{BH}/(v_{BH}^2 + c_S^2)$. As was studied in Paper I, this mechanism is able to reduce the binary separation to distances where gravitational radiation is efficient and will cause a merger within another 10^7 yr.

We found that gas plays an important role in the coalescence of the binary when the MBHs satisfy the observed m-σ_c relation and the disk thickness is of the order of tens of parsecs. This disk thickness is inferred from observations whenever gas is present in amounts greater than $10^8 M_{\odot}$; this corresponds, for an average spiral galaxy like the Milky Way, to only 0.1% of the total mass being in gas. Our work suggests that the MBH binary will merge within a few times 10^7 yr for the various values of the model parameters studied. Galaxies typically merge in 10^8 yr, and therefore these results imply that in a merger of galaxies with at least 1% of their total mass in gas, the MBHs will coalesce soon after the galaxies merge.

The final coalescence has crucial implications for possible scenarios of massive black hole evolution and growth. Our work supports scenarios of hierarchical buildup of massive black holes, which in their most recent versions (Kauffmann & Haehnelt 2000; Haehnelt 2004; Volonteri et al. 2003; Di Matteo

et al. 2003) assume that the first "seed" black holes appear at high redshifts ($z > 10$) with intermediate masses ($\sim 300\ M_\odot$) and that the black holes grow by mergers and gas accretion following the merger hierarchy from early times until the present. In particular, this result supports the assumption that halo mergers lead to black hole mergers when gas is present, something probably always true at high redshift. The final coalescence of the black holes leads to gravitational radiation emission that would be detectable up to high redshift by the *Laser Interferometer Space Antenna* (*LISA*; Haehnelt 2003). This is a promising way of assessing the role of mergers in black hole growth and evolution.

REFERENCES

Armitage, P., & Natarajan, P. 2002, ApJ, 567, L9
Artymowicz, P., & Lubow, S. H. 1994, ApJ, 421, 651
———. 1996, ApJ, 467, L77
Barnes, J. E. 2002, MNRAS, 333, 481
Barnes, J. E., & Hernquist, L. 1992, ARA&A, 30, 705
———. 1996, ApJ, 471, 115
Begelman, M., Blandford, R., & Rees, M. 1980, Nature, 287, 307
Chandrasekhar, S. 1943, ApJ, 97, 255
Di Matteo, T., Croft, R. A. C., Springel, V., & Hernquist, L. 2003, ApJ, 593, 56
Dopita, M. A. 1997, Publ. Astron. Soc. Australia, 14, 230
Downes, D., & Solomon, P. M. 1998, ApJ, 507, 615 (DS98)
Escala, A., Larson, R. B., Coppi, P. S., & Mardones, D. 2004, ApJ, 607, 765 (Paper I)
Goldreich, P., & Tremaine, S. 1982, ARA&A, 20, 249
Haehnelt, M. 2003, in AIP Conf. Proc. 686, The Astrophysics of Gravitational Wave Sorces, ed. J. M. Centrella (New York: AIP), 211
———. 2004, in Coevolution of Black Holes and Galaxies, ed. L. C. Ho (Cambridge: Cambridge Univ. Press) 406
Jogee, S., Scoville, N. Z., & Kenney, J. D. P. 2005, ApJ, 630, in press
Kauffmann, G., & Haehnelt, M. 2000, MNRAS, 311, 576
Kazantzidis, S., et al. 2005, ApJ, 623, L67

Lin, D. N. C., & Papaloizou, J. 1979, MNRAS, 186, 799
Makino, J., & Ebisuzaki, T. 1996, ApJ, 465, 527
Merritt, D., & Ferrarese, L. 2001, ApJ, 547, 140
Mestel, L. 1963, MNRAS, 126, 553
Mihos, C., & Hernquist, L. 1996, ApJ, 464, 641
Milosavljevic, M., & Merritt, D. 2001, ApJ, 563, 34
———. 2003, ApJ, 596, 860
Ostriker, E. 1999, ApJ, 513, 252
Peters, P. 1964, Phys. Rev., 136, 1224
Plummer, H. C. 1911, MNRAS, 71, 460
Quinlan, G. 1996, NewA, 1, 35
Richstone, D., et al. 1998, Nature, 395, A14
Sanders, D., & Mirabel, I. 1996, ARA&A, 34, 749
Springel, V., Yoshida, N., & White, S. 2001, NewA, 6, 79
Taniguchi, Y., & Wada, K. 1996, ApJ, 469, 581
Tremaine, S. et al. 2002, ApJ, 574, 740
Volonteri, M., Madau, P., & Haardt, F. 2003, ApJ, 593, 661
Wada, K. 2001, ApJ, 559, L41
Wada, K., & Norman, C. A. 2001, ApJ, 547, 172
Young, J. S., et al. 1995, ApJS, 98, 219